ELSEVIER

Chemical Physics 219 (1997) 173–191

Chemical Physics

Intermolecular potential for phenol based on the test particle model

Kritsana Sagarik [a,*], Prapasri Asawakun [b]

[a] School of Chemistry, Institute of Science, Suranaree University of Technology, Nakhon Ratchasima 30000, Thailand
[b] School of Mathematics, Institute of Science, Suranaree University of Technology, Nakhon Ratchasima 30000, Thailand

Received 16 December 1996

Abstract

An intermolecular potential to describe the interaction between phenol molecules was constructed using the test particle model (T-model). The T-model potential was used in the calculation of the equilibrium structures and energies of phenol dimers and trimers. The absolute and local energy minima on the T-model potential energy surface were examined by ab initio calculations with the second-order Møller–Plesset perturbation (MP2) theories. The equilibrium structures of phenol dimers computed from the T-model potential agree well with the MP2 results, and are compatible with those deduced from rotational coherence spectroscopy. The hydrogen bonds (H-bonds) in phenol–water 1:1 complexes were also investigated using the T-model potentials and MP2 calculations. The results are in good agreement with the previous ab initio calculations with a larger basis set and experiment in the gas phase. Structures and energies of liquid phenol, as well as phenol in aqueous solution, were studied using Molecular Dynamics (MD) and Monte Carlo (MC) simulations, respectively. The results are discussed in comparison with available theoretical and experimental results on the same and similar systems.

1. Introduction

Structures, energetics and dynamics of various types of molecular clusters have received much attention from molecular scientists since the knowledge of such complexes could lead to the understanding of the interactions in biological systems [1–3]. The advancement of spectroscopic techniques nowadays allows molecular spectroscopists to investigate structures and energies of small van der Waals complexes in the gas phase with reasonable accuracy [4,5]. The advancement of computer technology in the last decades has also allowed computational chemists to investigate small hydrogen-bonded (H-bonded) and van der Waals complexes with higher accuracy. The theoretical and experimental approaches are considered to play a supportive role in the study of small molecular clusters [6]. The situation for large molecular systems is, however, rather complicated. Reliable results cannot be obtained easily due to the difficulties in the experimental set-up and the complexities of the measured spectral properties. For the theoretical approach, the size of molecules limits ab initio calculations to the Hartree–Fock level of theory, in which the effects of the electron correlation are neglected. The molecular clusters considered are, therefore, restricted to those

* Corresponding author. E-mail: kritsana@alpha.sut.ac.th, asawakun@alpha.sut.ac.th

PII S0301-0104(97)00094-3

governed by electrostatic and dipole–dipole interactions, to which the conventional Hartree–Fock approximation can be applied reasonably well.

Molecular clusters formed from aromatic compounds have been a subject of interest since they represent the interaction between π-systems which are found in DNA and side chains of proteins. As the prototype of $\pi-\pi$ interaction, the benzene dimer seems to be the most popular choice to represent the interaction between π-systems. It has been selected as a model system both for spectroscopic and theoretical investigations [7–11]. A comprehensive review on structures of aromatic van der Waals clusters can be found in Ref. [12]. Since the electron correlation is one of the dominating factors in deciding the structures and energies of this type of molecular association, the theoretical methods applied to such systems must take into account the dispersion energy contribution properly, either in a direct or an approximate way. The construction of potential energy surfaces for such systems, using ab initio calculations with inclusion of the electron correlation in a direct method, is computationally demanding and still not practical at present.

An alternative computational method to compute the intermolecular potentials has been put forward [13,14]. It was called the test-particle model or briefly T-model since the main energy contributions to the total interaction energy are derived separately by probing molecules of interest with suitable test particles. This considerably reduces the computational effort since only three degrees of freedom are considered in the construction of intermolecular potentials, instead of six, as in the case of ab initio calculations in the supermolecular approach. The computed potential parameters of the T-model are considered to be site parameters and have been shown to be transferable [15]. Most importantly, the T-model potentials incorporate the effects of electron correlation in an approximate way. This makes the T-model potentials suitable for the investigation of large molecular clusters, in which the effects of electron correlation play a dominant role. The T-model potentials have been tested successfully in the calculations of equilibrium structures and interaction energies of a rather wide range of molecules, from diatomic molecules such as HF [15,16] to the base pairs of DNA [15]. The interaction between the π-systems in heterocyclic aromatic compounds like pyridine was also successfully studied using the T-model potential [17]. The T-model potentials have been proved to be applicable for the investigation of the condensed phase properties, both by Monte Carlo (MC) [16,17] and Molecular Dynamics (MD) simulations [17–20]. The previous results, together with the results for pyridine systems, show the potential of the T-model in further study of molecular interaction in other π-systems.

In the present work, the T-model potential was constructed for phenol and applied in the study of equilibrium structures and interaction energies of phenol dimers and trimers. The computed results were checked using ab initio calculations at MP2 (Møller–Plesset perturbation theory) level of theory. Structural, thermodynamic and dynamic properties of liquid phenol were investigated using MD. The structures of liquid phenol were discussed based on the pair correlation functions ($g(R)$). The phenol–water 1:1 complex was also investigated using the T-model and MP2 calculations. The structures of phenol in aqueous solution were derived from MC. The hydration patterns of phenol were analyzed using the computed probability distributions (PD) of oxygen (PDO) and hydrogen (PDH) atoms of water in the vicinity of a phenol molecule and illustrated by the PD maps. The hydration energies were discussed based on the averaged solute–solvent and solvent–solvent interaction energies.

2. The test-particle model (T-model) potential for phenol

The derivation of the T-model has been discussed in detail elsewhere [13]. Only some important aspects will be mentioned here. In the T-model, the total interaction energy (ΔE) between molecules A and B is written as a sum of the first-order interaction energy ($\Delta E^1_{\mathrm{SCF}}$) and the higher-order energy (ΔE^{r}),

$$\Delta E = \Delta E^1_{\mathrm{SCF}} + \Delta E^{\mathrm{r}} \tag{1}$$

$\Delta E^1_{\mathrm{SCF}}$ accounts for the exchange repulsion and electrostatic energies. $\Delta E^1_{\mathrm{SCF}}$ is computed from the

first-order SCF calculations and takes the following analytical form:

$$\Delta E^{1}_{\mathrm{SCF}} = \sum_{i\in A}\sum_{j\in B}\left[\exp\left(\frac{-R_{ij}+\sigma_i+\sigma_j}{\rho_i+\rho_j}\right)+\frac{q_i q_j}{R_{ij}}\right], \tag{2}$$

where ρ_i, σ_i and q_i are the site parameters, which are the properties of molecules A and B. R_{ij} are the site–site distances. All quantities in Eq. (2) are in atomic units. The exchange repulsion energy, represented by the exponential terms in Eq. (2), accounts for the size and shape of interacting molecules. ρ_i and σ_i are determined by probing molecules A, as well as B, with an uncharged spherical test particle. A nitrogen atom (N) in its average of terms state has been reported to be the most suitable [13]. The repulsion energies between A and N, as well as B and N, are computed starting from the wavefunctions of A and N, and B and N, respectively. Since molecules A and B are not necessarily spherically symmetric, molecules A and B must be probed by the test particle in all possible directions. For phenol, 1100 repulsion energies were computed to cover the repulsion part of the potential energy surface. The exponential parameters in Eq. (2) are determined initially for the interaction between A and N, as well as B and N, by means of least squares fits. With the aid of a combination rule [13], ρ_i and σ_i could be computed for molecules A and B. The point charges (q_i) can be determined in a similar way. The Coulombic interactions between A and B with a point charge (q) are calculated from the wavefunctions of A and B, respectively. The results are the electrostatic potentials in the vicinity of A and B. q_i are determined to reproduce the electrostatic potentials. This is similar to the charges computed from the Potential Derived (PD) method [21,22].

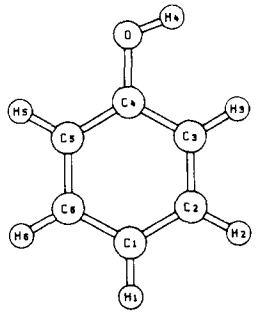

Fig. 1. Geometry of phenol with atom numbering system.

Table 1
Parameters for the T-model potential of phenol (in au)

Atom	σ_i	ρ_i	q_i
O	1.122591	0.248594	−0.667863
C1	1.201071	0.277213	−0.202844
C2	1.276142	0.236488	−0.053883
C3	1.091620	0.358983	−0.504382
C4	1.278229	0.172507	0.602824
C5	1.189580	0.295535	−0.352276
C6	1.053884	0.339821	−0.171089
H1	−0.067537	0.331718	0.138852
H2	−0.013789	0.303927	0.165180
H3	0.040251	0.262547	0.199031
H4	−0.177958	0.267606	0.452293
H5	0.017042	0.278423	0.205855
H6	−0.004693	0.284322	0.188302

$C_6 = 1.43$ for phenol–phenol interaction.
$C_6 = 0.70$ for phenol–water 1:1 complex.

The molecular geometry of phenol with the atom numbering system is shown in Fig. 1. The basis sets used in the repulsion and electrostatic energy calculations were taken from Ref. [17]. ρ_i, σ_i and q_i for phenol are given in Table 1. The point charges in Table 1 yield the dipole moment of 1.41 D, about 13% larger than the experimental value [23]. The dipole moment computed from ab initio SCF calculations with 6-31G*(5D) basis set was reported to be 1.45 D [24].

The higher-order energy (ΔE^{r}) in Eq. (1) represents the dispersion and polarization parts of the T-model potential. It is approximated as

$$\Delta E^{\mathrm{r}} = -\sum_{i\in A}\sum_{j\in B} C^{6}_{ij} F_{ij}(R_{ij}) R^{-6}_{ij} \tag{3}$$

where

$$F_{ij}(R_{ij}) = \exp\left[-\left(1.28\, R^{0}_{ij}/R_{ij} - 1\right)^{2}\right], \quad R_{ij} < 1.28\, R^{0}_{ij}$$
$$= 1, \text{ elsewhere}. \tag{4}$$

R^{0}_{ij} in Eq. (4) is the sum of van der Waals radii of the corresponding atoms. $F_{ij}(R_{ij})$ is a damping function applied to correct ΔE^{r} at small R_{ij}. C^{6}_{ij} are adjustable parameters. C^{6}_{ij} can be computed from the Slater–Kirkwood relation as follows:

$$C^{6}_{ij} = C_6 \frac{3}{2}\frac{\alpha_i \alpha_j}{\left(\alpha_i/N_i\right)^{1/2} + \left(\alpha_j/N_j\right)^{1/2}}, \tag{5}$$

where α_i denotes the atomic polarizability and N_i is the number of valence electrons of the corresponding atoms. For ΔE^r, only C_6 is the unknown. The value of C_6 can be determined in many different ways. Since the experimental second virial coefficient ($B(T)$) is available for phenol [25], C_6 was determined in the present work by a fit of the incomplete potential, including ΔE^1_{SCF}, to the experimental $B(T)$. C_6 was computed to be 1.43 for phenol–phenol interaction.

It should be noted that the adjustment of C_6 to reproduce the experimental $B(T)$ allows the T-model potential to be calibrated. This makes the T-model potential more realistic in comparison with the potentials derived purely from ab initio calculations. To our experience, if there is no experimental $B(T)$ available, one may calibrate the T-model potential to the properties related to the molecular interaction. This includes the thermodynamic properties, such as the experimental or theoretical dimerization energies, and dynamic properties such as the experimental diffusion or viscosity coefficients.

3. Phenol dimers, trimers and phenol–water 1:1 complexes

The T-model potential computed in the previous section was used in the calculation of the equilibrium structures and interaction energies of phenol dimers and trimers. The minimum energy geometries for the dimers and trimers were searched by placing a phenol monomer at the origin of the Cartesian coordinate system. The starting coordinates of the second as well as the third phenol molecule were chosen at random. Based on the T-model potential, the corresponding nearest energy minima were located using a minimization technique. About 100 starting configurations were generated for both dimers and trimers. For the phenol dimer, at least seven distinct lowest-lying minimum energy geometries were predicted. They are shown in Fig. 2, together with the corresponding interaction energies (ΔE) and some selected atom–atom distances.

The absolute minimum energy geometry for the phenol dimer was found to be a H-bonded structure, the dimer A in Fig. 2. The O...O distance and the ∠O...O–H4 angle, involved in the H-bond formation, are 2.97 Å and 6.25°, respectively. The ∠O...O–H4 not involved in H-bond formation was predicted to be 138.23°. The interaction energy for the dimer A was computed by the T-model potential to be −31.31 kJ/mol. The equilibrium structures of phenol dimer were investigated experimentally in the gas phase using rotational coherence spectroscopy [26]. From the analysis of the rotational constants, the authors suggested the most probable dimer structure, regarded as Structure I. Structure I is virtually the same as the dimer A in the present study, with a slightly longer O...O distance, 3.05 Å. The O...H4–O H-bond was constrained in the analysis to be strictly linear. The ∠O...O–H4, not involved in H-bond formation, was found to be slightly smaller than the present result, 131.7°. However, the uncertainties in the experimental results were estimated in Ref. [26] to be ±0.2 Å and 20°, for the distances and angles, respectively. A similar dimer structure called herringbone structure was found to be the most stable for pyridine [17]. Structure I and the herringbone structure, as well as the dimer A, are expected as the result of the balance between the H-bond and the π–π interactions.

As mentioned earlier, the structure and interaction energy of benzene dimer in the gas phase have been a subject of theoretical and experimental investigations since it represents the prototype for the π–π interaction. There were at least four dimer structures suggested by ab initio calculations and experiments to exist in the gas phase namely, parallel displaced, T-shaped, parallel staggered and herringbone structures [12]. Among these dimer structures, the existence of the T-shaped and parallel displaced structures in the gas phase seems to be the most popular topic considered in experiments [12]. Recent ab initio calculations with various sizes of the basis set [11] showed that the parallel displaced structure is the lowest-energy structure, whereas the T-shaped structure is the low-energy saddle point for interconversion between parallel displaced structures. A tilted T-shaped structure, similar to the herringbone structure, was reported in Ref. [11] to be just a shallow minimum energy geometry. Based on the present results and our experience on pyridine system [17], it is reasonable to believe that all of the four structures could exist in the gas phase. However, since the ab initio calculations [11] have shown that the potential

energy surface of benzene is quite flat, more accurate experimental methods must be devised to distinguish the four structures.

Another H-bonded dimer (the dimer B in Fig. 2), in which the phenyl moieties lie in the same plane and trans to each other, was predicted by the T-model potential to be less stable than the dimer A. The O...O distance in this case is 2.97 Å with the H-bond energy of −28.72 kJ/mol. The dimer C was predicted by the T-model potential to be slightly less stable than B. It is represented by cyclic O–H4...O H-bonds, with both phenyl moieties cis to the O...O axis. This binding feature is expected to possess the highest π–π interaction. The π–π attractive interaction energy is, however, partially cancelled out by the repulsion between the π electrons and atomic nuclei in the different phenyl rings. This makes the dimer C less stable than A and B. The O...O distance and interaction energy for the dimer C are 2.74 Å and −27.13 kJ/mol, respectively. The existence of the dimers B and C in the gas phase was discussed in Ref. [27]. It was pointed out in Ref. [26] that these dimer structures are inconsistent with their experimental rotational constants. Based on the computed interaction energies and the fact that phenol has a dipole moment of 1.22 D [23], we expect both dimer structures to exist in the gas phase. The stability of the dimer D is comparable with C. It shows a bent T-shaped structure, consisting of two binding sites, namely the C3–H3...O H-bond and the O–H4...X. X in this case labels the center of the phenyl ring. The O–H4...X interaction could be regarded as a type of H-bonding, in which the π-electrons on the phenyl ring act as the proton acceptor. This type of H-bond interaction was already found in the case of benzene–water 1:1 complex, in which water acts as a proton donor pointing hydrogen atoms toward the π electron cloud [7,28,29]. The cyclic H-bonds in the dimer E are similar to C. The geometry of the dimer E was reported in Ref. [26] to be compatible with the observed rotational constants. The dimer E is slightly less stable than C due to the lack of the π–π attractive interaction. The shape of the dimer F is similar to D, with the interaction energy of −24.10 kJ/mol. Only the O–H4...X interaction is responsible for this dimer structure. The dimer G represents the least stable structure in this series, with two C3–H3...O–H4 cyclic H-bonds and the interaction energy of −21.56 kJ/mol.

The stability order for the phenol dimers deduced from the T-model potential can be summarized as follows:

$$A > B > C \geqslant D > E > F > G$$

In order to sample check the above stability order, some of the dimer structures predicted by the T-model potential were recomputed using ab initio calculations with supermolecular approach. Since a portion of the interaction energies of phenol dimers is from the π–π interaction, which is the result of the electron correlation in the phenyl moieties, ab initio calculations had to be made at the level of theory higher than the Hartree–Fock approximation. It should be noted that ab initio calculations with a sufficiently large basis set beyond the Hartree–Fock level on phenol dimers are very CPU time consuming, even with current computer technology. The strategy in the present study was, therefore, to compromise between the accuracy and availability of computer resources. After several trial ab initio calculations, we found that the calculations at the MP2 level with a Double-Zeta (DZ) basis set were the most appropriate choice for us. A remark should be made on ab initio calculations. It is well known that ab initio calculations of molecular clusters with a restricted size of the basis set in a supermolecular fashion, as done in the present section, suffer from Basis Set Superposition Error (BSSE). Since the size of the basis set selected in the present case was still far from the complete basis set (CBS) limit, the computed interaction energies of phenol dimers included the BSSE. In order to partly solve the BSSE problem, counterpoise corrections (CC) were applied for all MP2 interaction energy calculations, with the hope that at least the relative stability order of the interaction energies could be predicted correctly. It should further be stressed that the T-model and the MP2 are obviously based on different theories. Therefore, one should not expect exactly the same potential energy surface from both methods. The main aim for MP2 calculations here was only to investigate the trends of the interaction energies on the MP2 potential energy surface both with and without the counterpoise correction and, especially, in the vicinities of the T-model energy minima.

In order to maintain reasonable CPU time, only the first four dimer structures in the above stability order were reinvestigated using MP2 calculations. The dimer structures were reoptimized partially starting from the coordinates predicted by the T-model potential, by variations of a selected characteristic distance between each monomer. The counterpoise corrected and uncorrected SCF and MP2 interaction

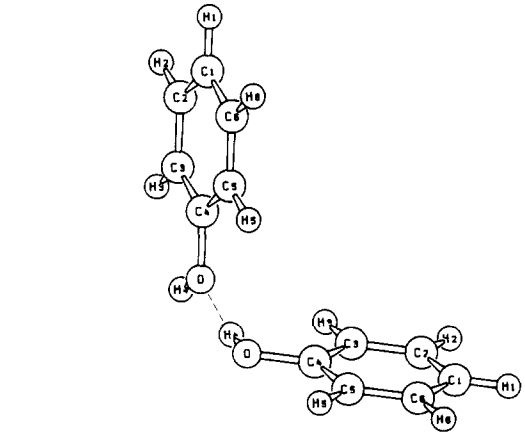

-A-

ΔE	-31.31
O-O	2.97
O-H4	2.03
	3.72
C1-C1	7.98
C4-C4	4.29
O-O-H4	6.25
	138.23

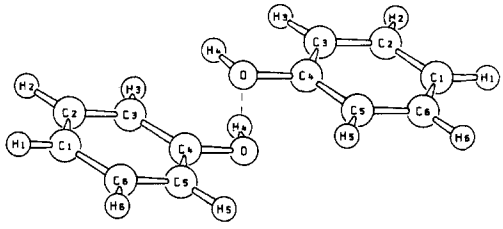

-B-

ΔE	-28.72
O-O	2.97
O-H4	2.03
	3.74
C1-C1	9.78
C4-C4	4.69
O-O-H4	4.62
	140.62

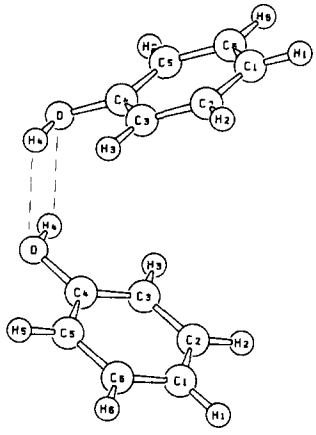

-C-

ΔE	-27.13
O-O	2.74
O-H4	2.25
	2.31
C1-C1	6.45
C4-C4	3.95

Fig. 2. Energy optimized phenol dimer geometries and interaction energies (ΔE in kJ/mol) as well as selected characteristic distances (in Å) and angles (in °) derived from the T-model potential. X = center of the phenyl ring.

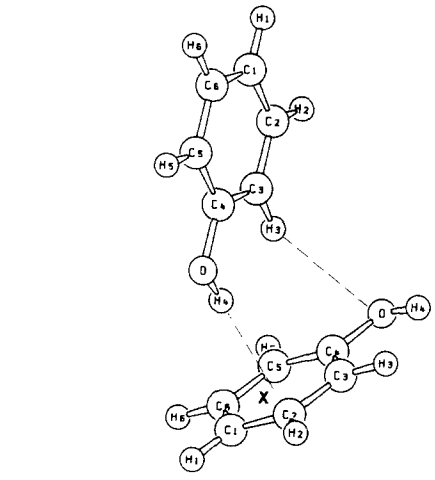

-D-

ΔE	-27.12
O-H3	2.88
	4.11
O-X	3.40

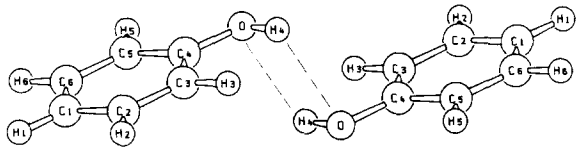

-E-

ΔE	-25.15
O-O	2.78
O-H4	2.31
	2.31
C1-C1	9.50
C4-C4	4.41

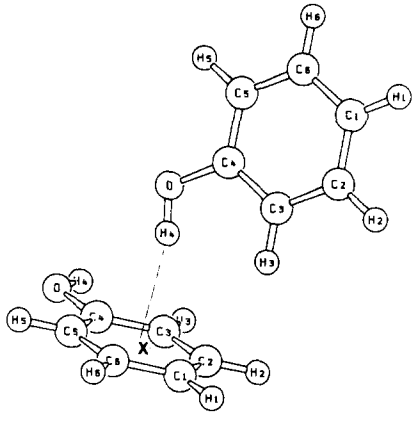

-F-

ΔE	-24.10
O-O	3.97
O-X	3.30
H4-X	3.21

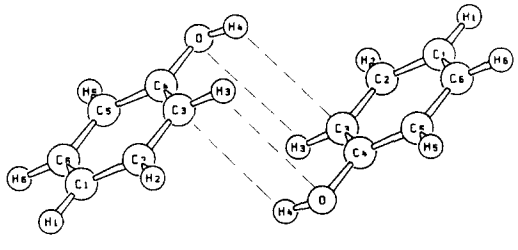

-G-

ΔE	-21.56
O-O	4.50
O-H3	2.95
	2.95
O-C3	3.36
	3.36

Fig. 2 (continued).

energies, in the vicinities of the T-model minima are regarded as SCF(CC), SCF, MP2(CC) and MP2, respectively. They are compared in Table 2. Table 2 shows the interaction energies when the characteristic distances were varied from the T-model results.

The stability order for the MP2 and MP2(CC) calculations was found to be as follows.

MP2: A > B > C > D

MP2(CC): A ≥ B > C > D

The stability orders computed for the MP2 and MP2(CC) are not different from the T-model potential. MP2 predicted the interaction energy of the dimer A to be −44.72 kJ/mol, in comparison with −22.95 kJ/mol by MP2(CC). This is not surprising since the counterpoise corrected interaction energy represents the upper boundary of the interaction energies. The characteristic distances deduced from MP2 and MP2(CC) deviate from the T-model results within the experimental error estimated in Ref. [26], except for the dimer D, in which the MP2(CC) yielded the O...X distances about 0.3 Å longer than the T-model. The counterpoise corrected distances seem to be systematically longer than the uncorrected values. This is in line with the results in Ref. [30], in which the application of the counterpoise correction in SCF, MP2 and MP4 calculations led to a systematic extension of the R_{FF} H-bond of HF dimer, in comparison with the uncorrected distances. The R_{FF} converges to the experimental value when the basis set was extended to the CBS limit for all levels of theory.

The T-model potential predicted an absolute and several local minimum energy geometries for the trimers. Three of them are illustrated in Fig. 3. The absolute minimum energy geometry is represented by a cyclic arrangement of O–H...O H-bonds, the trimer A in Fig. 3. The O–H...O H-bond distances are all equal, 2.89 Å, with the interaction energy of −80.75 kJ/mol. The ∠O...O–H4 angles involved in H-bond formation are all the same, 25.20°. This H-bond arrangement is similar to that found in water [31] and HF [32] trimers. For the trimer B, the cyclic O–H4...C2–H2 as well as the O...H4–O and O–H4...X H-bonds are responsible for the stability. The interaction energy in this case is −75.60 kJ/mol. The trimer C consists of two O–H4...O H-bonds and a π–π interaction, with the interaction

Table 2
The interaction energies (ΔE) when the selected characteristic distances varied from the T-model results

Dimer A					Dimer B				
ΔO...O (Å)	ΔE (kJ/mol)				ΔO...O (Å)	ΔE (kJ/mol)			
	MP2	MP2(CC)	SCF	SCF(CC)		MP2	MP2(CC)	SCF	SCF(CC)
−0.20	−44.55	−20.27	−28.55	−16.08	−0.20	−39.71	−20.50	−28.27	−18.21
−0.10	−44.72 [a]	−22.30	−29.70	−18.12	−0.10	−39.84 [a]	−22.18	−29.10 [a]	−19.75
0.00	−43.78	−22.95 [a]	−29.81 [a]	−18.89 [a]	0.00	−38.89	−22.54 [a]	−28.93	−20.10 [a]
0.10	−42.13	−22.74	−29.11	−18.87	0.10	−37.24	−22.10	−27.98	−19.71
0.20	−40.03	−22.00	−28.04	−18.36	0.20	−35.16	−21.19	−26.71	−18.91
Dimer C					Dimer D				
ΔO...O (Å)	ΔE (kJ/mol)				ΔO...X (Å)	ΔE (kJ/mol)			
	MP2	MP2(CC)	SCF	SCF(CC)		MP2	MP2(CC)	SCF	SCF(CC)
−0.30	−21.98	3.82	−2.48	10.45	−0.10	−23.78	−7.41	−4.87	3.61
−0.20	−28.43	−5.23	−11.33	0.73	0.00	−24.03 [a]	−10.08	−8.02	−0.64
−0.10	−31.59	−10.67	−16.65	−5.30	0.10	−23.42	−11.62	−9.85	−3.54
0.00	−32.56 [a]	−13.71	−19.49	−8.88	0.20	−22.82	−12.35	−10.84	−5.45
0.10	−32.09	−15.17	−20.58	−10.84	0.30	−20.86	−12.53 [a]	11.14 [a]	−6.65
0.20	−30.73	−15.59 [a]	−20.61 [a]	−11.72	0.40	−19.28	−12.36	−11.03	−7.34
0.30	−28.82	−15.37	−19.94	−11.92	0.50	−17.69	−11.99	−10.68	−7.68

[a] Minimum energy.
X = center of the phenyl ring.

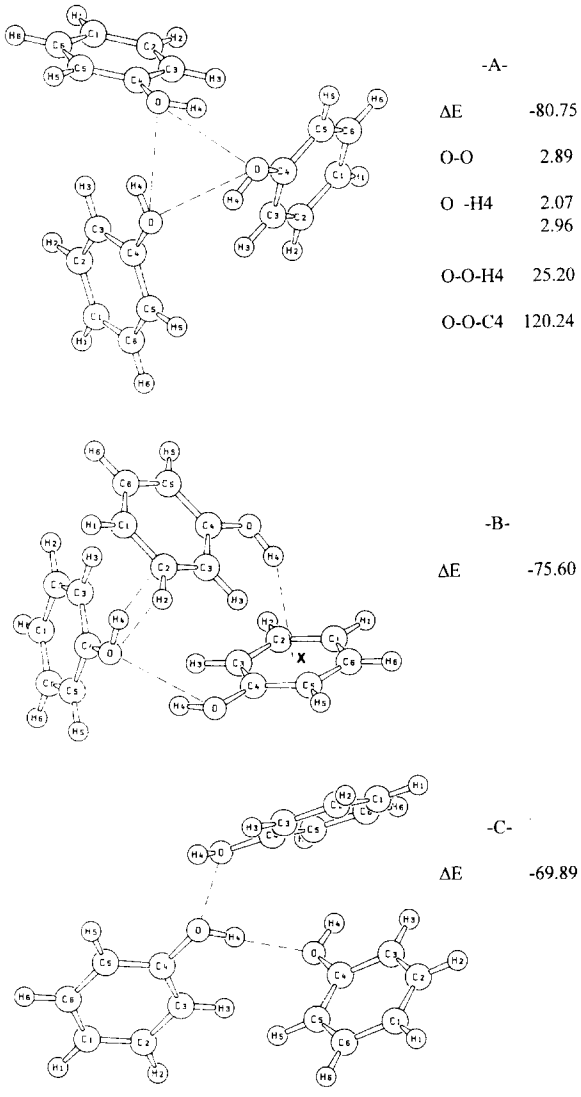

Fig. 3. The most stable phenol trimer geometries and interaction energy (ΔE in kJ/mol) as well as selected characteristic distances (in Å) and angles (in °) obtained from the T-model potential. X = center of the phenyl ring.

energy of −69.89 kJ/mol. The absolute minimum energy geometry of the phenol trimer (the trimer A) discussed in the present section confirmed the results of a vibrational spectroscopic experiment reported in Ref. [33], in which a cyclic arrangement of O–H...O H-bonds was found to exist in the supersonic jet-cooled molecular beam.

It should be noted that Ramondo et al. [34] studied the effects of intermolecular O–H...O H-bonds on the molecular structure of phenol using ab initio calculations at the Hartree–Fock level of theory with a 6-31G* basis set. The systems investigated were eight phenol–water 1:1 complexes, as well as phenol dimer and trimer. Since the main aim of Ref. [34] was only to study changes in the phenol monomer geometry especially in the solid state, the geometry optimizations of the dimer and trimer were made starting from the structures derived from X-ray data, with various constraints on the intermolecular geometrical parameters. The dimer selected in the investigation was between the dimer A and B in the present study. The trimer in the solid state was similar to the trimer C in Fig. 3. The authors pointed out that the formation of the O–H...O H-bonds affect the geometry of the O–H group and the ipso region of the benzene ring. Since there were no energy values reported in Ref. [34], further comparison with the present results could not be made.

As mentioned earlier, the T-model parameters in Eq. (2) are site parameters. Therefore, the potential energy surface describing the interaction between phenol and other molecules with known T-model parameters could be constructed, provided that the C_6 parameter is known. To our experience [15–18], the C_6 parameter could be varied about 10% from its optimal value without leading to any significant change in the computed equilibrium geometries, and the value for the interaction between water and various model biomolecules could be set to 0.70 [35]. In the present study, the T-model potentials for phenol and water [15] were applied to investigate the H-bond in phenol–water 1:1 complexes. In order to locate the absolute and local minimum energy geometries for phenol–water 1:1 complexes, a phenol molecule was fixed at the origin of the Cartesian coordinate system. The coordinates of a water were chosen randomly and the nearest energy minima were searched using the same procedure as for the phenol dimers. Three lowest-lying minimum energy geometries of phenol–water 1:1 complexes were predicted by the T-model potentials and are shown in Fig. 4. The MP2 calculations were also made to investigate all the three phenol–water 1:1 complexes using the DZ basis set. Additionally, each atomic basis set was augmented in this case with a polarization function (DZP). The geometries of phenol–water 1:1 complexes were optimized by variations of the

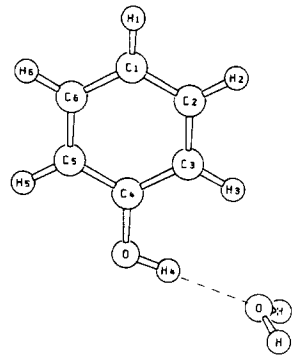

-A-

ΔE	-25.90
O-O	2.97
θ1	0.89
θ2	158.44

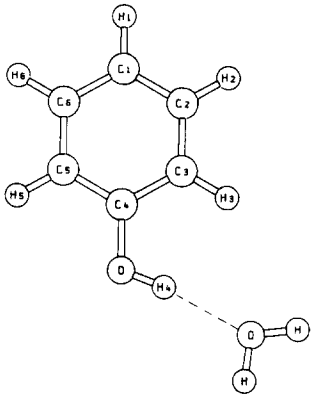

-B-

ΔE	-24.67
O-O	2.97
θ1	5.07
θ2	160.96

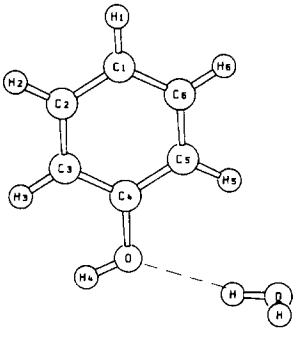

-C-

ΔE	-14.11
O-O	3.17
θ1	20.81
θ2*	161.61

Fig. 4. Energy optimized phenol–water 1:1 complex geometries and interaction energy (ΔE in kJ/mol) as well as the O...O distances (in Å) and $\theta 1$, $\theta 2$ and $\theta 2^*$ (in °) obtained from the T-model potential. $\theta 1 = \angle$O...O–H; $\theta 2$ = angle between O...O axis and the dipole moment vector of water; $\theta 2^*$ = angle between O...O axis and the vector bisecting the ∠H4–O–C4 angle.

O–H...O H-bond, starting from the T-model results. The BSSE for the phenol–water 1:1 complexes was corrected using the counterpoise correction. The BSSE corrected and uncorrected results for both MP2 and SCF are listed in Table 3. Table 3 shows deviations of the O–H...O H-bond distances from the T-model results.

The dimer in which water acts as a proton acceptor was predicted by the T-model potential to be the absolute minimum, with the O–H4...O H-bond length and energy of 2.97 Å and −25.90 kJ/mol, respectively (see the dimer A in Fig. 4). The molecular plane of water in this case is perpendicular to that of phenol. The ∠O...O–H4 angle and the angle between the O...O axis and the dipole moment vector of water ($\theta 1$ and $\theta 2$ in Fig. 4) were predicted by the T-model potentials to be about 1 and 158°, respectively. The O–H...O distance, $\theta 1$ and $\theta 2$ for water dimer were reported to be 2.99, 1.0 and 143.1°, respectively [36]. The phenol–water 1:1 complex was investigated using spectroscopic and molecular beam experiments in the gas phase, as well as ab initio calculations at MP2 level of theory [37]. The absolute minimum energy geometry for phenol–water 1:1 complex was reported to be the same as ours. Ab initio calculations at MP2 level with the 6-311 + + G(d,p) basis set and the counterpoise correction yielded an H-bond energy of −25.41 kJ/mol and an O...O distance of 2.94 Å, respectively. $\theta 1$ and $\theta 2$

Table 3
The interaction energies (ΔE) when the O...O distances deviated from the T-model results

	ΔO...O (Å)	ΔE (kJ/mol)			
		MP2	MP2(CC)	SCF	SCF(CC)
Dimer A	−0.30	−43.21	−22.05	−29.63	−17.50
	−0.20	−44.56 [a]	−25.49	−32.97	−21.79
	−0.15	−44.52	−26.40	−33.78	−23.06
	−0.10	−44.13	−26.90	−34.15 [a]	−23.88
	0.00	−42.62	−26.96 [a]	−33.95	−24.49 [a]
	0.10	−40.50	−26.17	−32.89	−24.14
Dimer B	−0.20	−38.43	−23.79	−28.75	−20.05
	−0.15	−38.48 [a]	−24.57	−29.57	−21.21
	−0.10	−38.20	−24.97 [a]	−29.97 [a]	−21.96
	0.00	−36.94	−24.92	−29.86	−22.48 [a]
	0.10	−35.09	−24.10	−28.94	−22.11
Dimer C	−0.30	−31.72	−9.40	−20.27	−7.25
	−0.25	−31.87 [a]	−10.37	−21.03	−8.42
	−0.20	−31.77	−11.06	−21.50	−9.30
	−0.15	−31.48	−11.51	−21.73	−9.91
	−0.10	−31.03	−11.75	−21.77 [a]	−10.30
	0.00	−29.77	−11.81 [a]	−21.41	−10.61 [a]
	0.10	−28.17	−11.47	−20.62	−10.48

[a] Minimum energy.

were computed to be 3.3 and 147.7°, respectively. The results are in excellent agreement with the present T-model results. The dimer structure, in which the molecular planes of phenol and water are coincident, was predicted by the T-model potential to be slightly less stable than the absolute minimum energy geometry. The interaction energy in this case is −24.67 kJ/mol, with the same O...O distance. $\theta 1$ and $\theta 2$ in this case are 5 and 161°, respectively. The dimer structure in which water acts as a proton donor is the least stable, with the O–H....O H-bond distance and energy of 3.17 Å and −14.11 kJ/mol, respectively. In Table 3, it is seen that the MP2, MP2(CC), SCF and SCF(CC) predicted the same stability order for phenol–water 1:1 complexes namely, the dimer A is more stable than B and C, respectively. The general trend discussed above was found when Tables 2 and 3 were compared namely, the counterpoise corrected O...O distances are systematically longer than the uncorrected ones, both at the MP2 and SCF level of theories. Both SCF(CC) and MP2(CC) yielded almost the same O...H–O H-bond distances as the T-model potential. The MP2, however, tends to give shorter O...H–O H-bond distances, in comparison to the SCF(CC), MP2(CC) and the T-model potentials. Feller and Feyereisen [38] investigated the structures and energies of the H-bonding in phenol–water 1:1 complexes using ab initio calculations both at the SCF and MP2 levels, with various sizes of the basis sets and the counterpoise correction. The authors focused their attention on four different dimer geometries. The lowest-energy geometry was predicted to be the same as the dimer A in Fig. 4, with the interaction energies at the MP2 level ranging from −25.50 to −27.58 kJ/mol. The dimer in which water acts as a proton donor, similar to the dimer C in the present study, was predicted to possess interaction energies ranging from −14.63 to −15.88 kJ/mol, in excellent agreement with the T-model potential.

From the results presented in this section, one can conclude that the T-model potentials predicted the equilibrium structures and interaction energies for both phenol dimer and trimer, as well as phenol–water 1:1 complexes in excellent agreement with all available experimental and theoretical estimates, and the T-model potentials can be applied in the investigation of liquid properties with confidence.

4. Monte Carlo (MC) simulations of a phenol molecule in aqueous solutions

Solvation of phenol in aqueous solution was modeled by placing a phenol molecule in the middle of a cubic box subject to periodic boundary conditions. The molecular plane of phenol was assumed to coincide with the XY plane of the box (with $Z = 0$ Å). 122 water molecules were fitted in the box. The density of water was maintained at 1 g/cm^3. The box length corresponding to the density is 15.5 Å. The cut-off radius was selected to be half of the box length and the Ewald summation was employed in the electrostatic energy calculations. In the course of MC, the ratio of accepted:rejected configurations was adjusted to the value of 0.5 by continuous adaptation of the maximum displacement and maximum rotational angles of each water molecule. The solvent–solvent interaction energies were computed based on the T-model potential reported in Ref. [15]. MC simulations on pure liquid water at 298 K with the T-model potential [15] yielded the averaged liquid potential energy of −34.03 kJ/mol, in comparison with −35.53 kJ/mol from the MCY (Matsuoka, Clementi and Yoshimine) potential [39]. In the present study, one million MC steps were devoted to the equilibration of the system at 298 K and another one million to the property calculation. The hydration structures analysed in the present study were based on the methods employed by Clementi et al. [39], in which the oxygen (PDO) and hydrogen probability distribution (PDH) maps were computed separately for water molecules. In this method, the volume above the molecular plane of a solute molecule is divided into layers of equal thickness. In the present case, three layers with the thickness of 1 Å were constructed. The layer with Z between 0 and 1 Å, 1 and 2 Å and 2 and 3 Å will be regarded as the bottom, middle and top layers, respectively. In each layer, the PDO and PDH were computed at the 60×60 grid intersections, by tracing the coordinates of oxygen and hydrogen atoms of water in the course of MC runs. They were represented by contour lines on the maps. The minimum and maximum contour lines, as well as the contour intervals, were the same for all PDO and PDH maps. Therefore, the density of the contour lines can be directly correlated to the probability density. In order to identify water

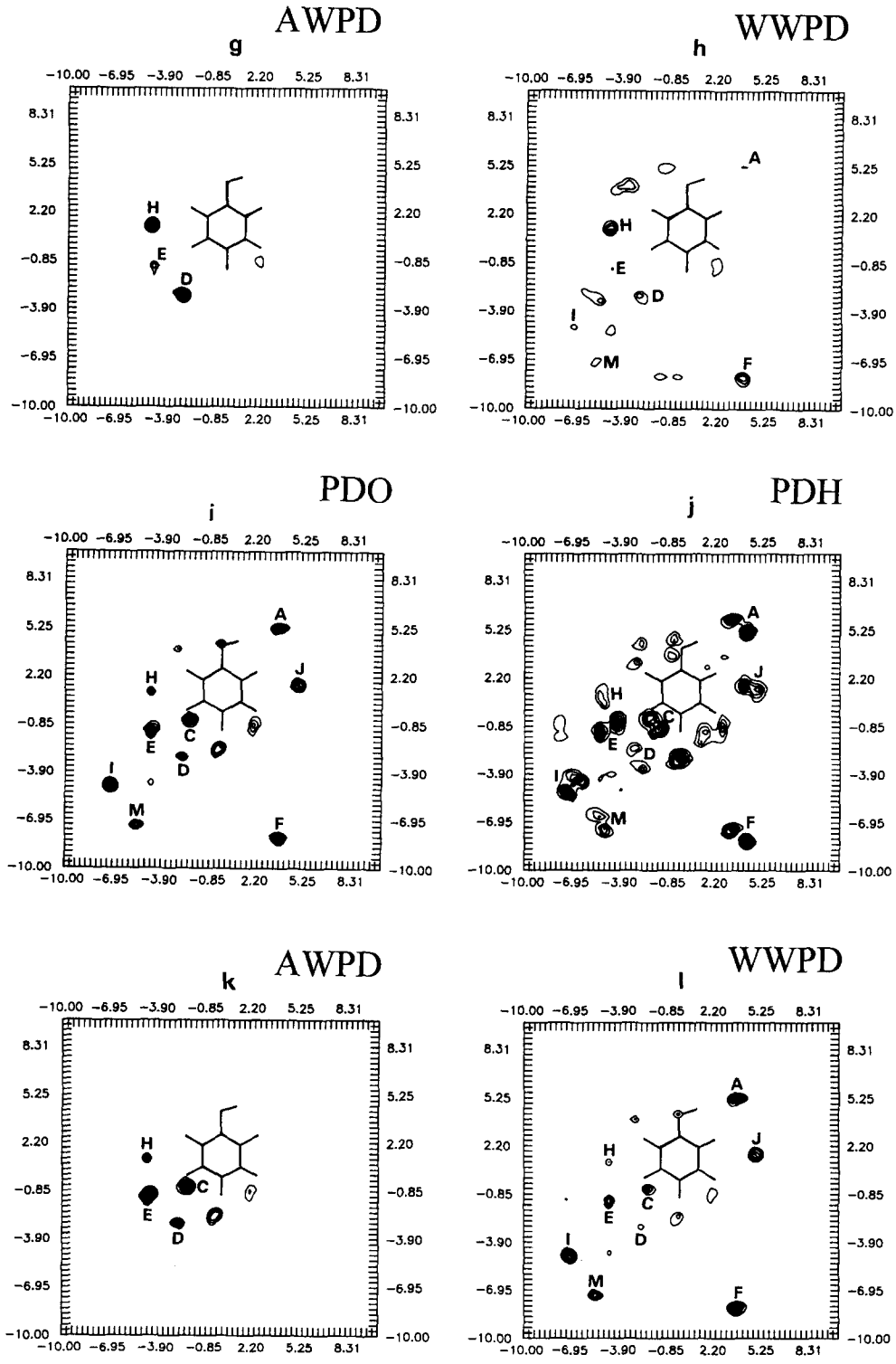

Fig. 5 (continued).

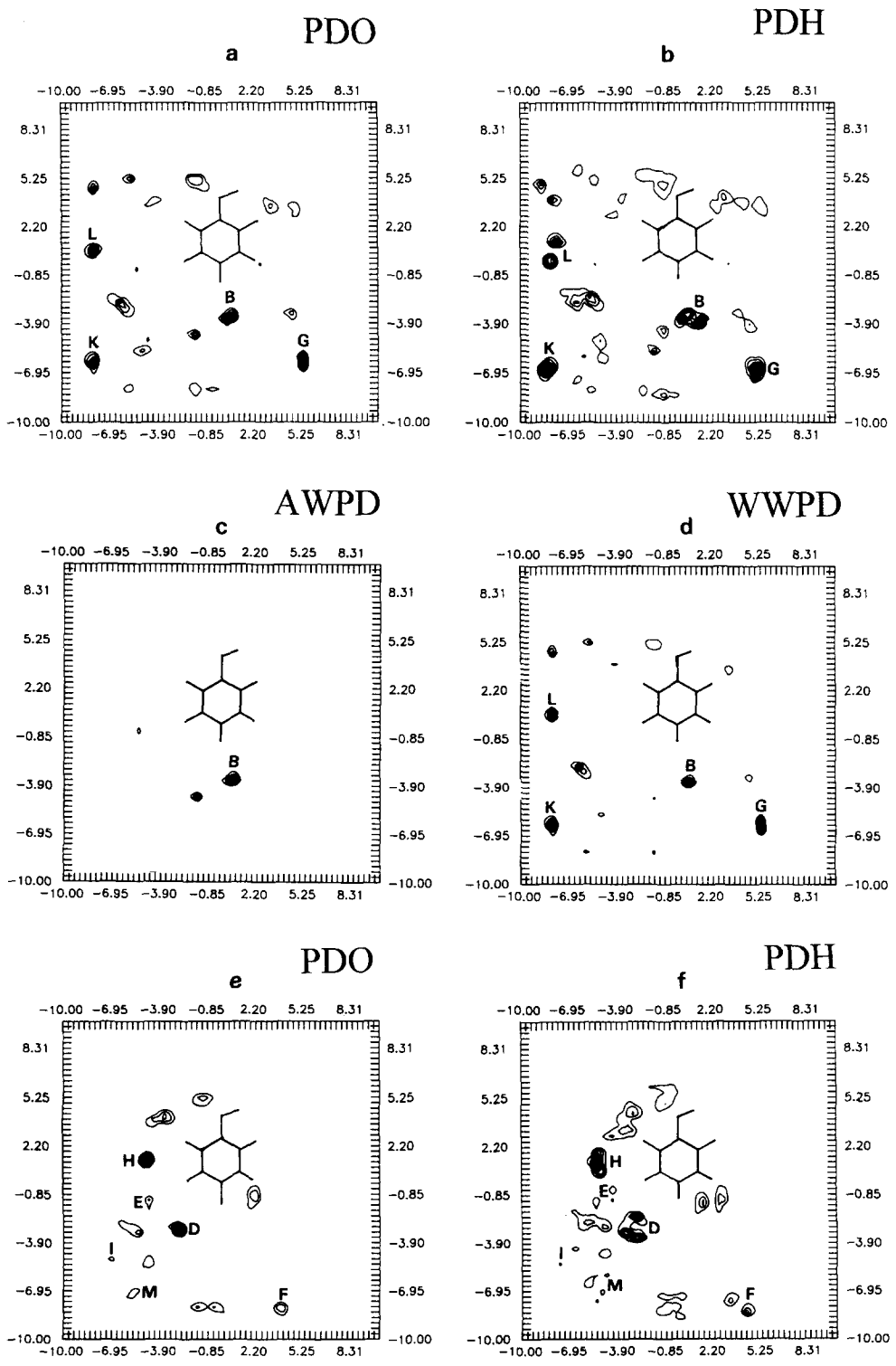

Fig. 5. PDO, PDH, AWPD and WWPD for phenol in aqueous solution computed from the MC simulations at 298 K (X and Y axes in Å). (a–d) for the bottom layer ($Z = 0$–1 Å); (e–h) for the middle layer ($Z = 1$–2 Å); (i–l) for the top layer ($Z = 2$–3 Å).

molecules in the hydration shells of phenol, some high-density contour areas on the PD maps were labeled, with A, B and C, respectively. A labels the area on PDO maps with the highest probability of finding oxygen atom of water, compared to B and C, respectively. The corresponding contour areas on the PDH maps were labeled using the same alphabets. The energy PD maps were also constructed to represent the averaged solute–solvent and solvent–solvent interaction energies in the same manner. They were regarded as AWPD and WWPD maps, respectively. Only negative energies are shown on the maps. These two energy maps illustrate the probability that a given water molecules could be 'bound' directly to the phenol or just 'caged' to a specific site by its neighbouring water molecules, respectively [40]. The areas on AWPD and WWPD maps were labeled according to the PDO maps. All the PD maps are shown in Fig. 5.

At equilibrium, the averaged total potential energy of phenol in aqueous solution was computed to be -54.83 kJ/mol at 298 K, 20.80 kJ/mol lower than the potential energy of pure liquid water discussed above. The averaged solute–solvent and solvent–solvent interaction energies are -13.73 and -40.57 kJ/mol, respectively. Molecular dynamics results were presented for phenol at the water liquid–vapor interface at 300 K [41]. The system studied contained a phenol molecule and 500 water molecules with the periodic boundary conditions applied in the three directions. The water–water and phenol–water interactions were described by TIP4P and Amber potentials, respectively. The free energy of adsorption was computed to be -11.7 ± 1.7 kJ/mol, in comparison with the experimental value, quoted in Ref. [41], of -15.9 kJ/mol. The free energy of hydration of benzene is known to be -3.2 kJ/mol [42]. The previous results indicate that the averaged solute–solvent interaction energy derived from MC is in a reasonable range.

Although the discussion on the hydration structure of phenol is made above the molecular plane, it is expected that a similar situation should be found if the analysis is made under the molecular plane due to the symmetry of phenol (C_s). Water molecules tend to concentrate on the top layer, about 2–3 Å above the phenol molecular plane. The highest probability of finding water, labeled with A, was found on the PDO map in this layer, see Fig. 5i. Superimposing the PDO map with the corresponding PDH map (Fig. 5j) shows the averaged orientation of the water molecule at A. The water molecule acts in this case as a proton acceptor H-bonding to O–H4 of phenol, similar to the dimer B in Fig. 4. The corresponding AWPD and WWPD maps (Fig. 5k and 5l) show that the solvent–solvent interaction or caging effect is mainly responsible for this averaged configuration. Water also prefers to stay in the area near H1 of phenol in the bottom layer. This area was labeled with B in Fig. 5a. The water molecule at B acts as a proton acceptor H-bonding at C1–H1 of phenol. AWPD and WWPD maps show that both solute–solvent and solvent–solvent interactions are responsible for this averaged configuration (see Fig. 5c and 5d). Another water molecule was found above H6 of phenol, labeled with C in the top layer. The water molecule at C acts as a proton acceptor and binds directly at H6 from above. It is only partially caged by its neighbouring water molecules (see AWPD and WWPD maps in Fig. 5k and 5l). Both hydrogens of water at C seem to be free to move in comparison with A and B. A water molecule, labeled with D in Fig. 5e and 5f, is localized in the area between H1 and H6 of phenol in the middle and top layers. The water molecules at B, D, C, E and H form a three dimensional network, spanning from H1, H6 to H5 of phenol. They are bound together with H-bonds and may be regarded as the water molecules in the first hydration shell. A and J form another network at H4 and H3 above the molecular plane. They can be included in the first hydration shell. A water molecule is seen near the oxygen atom of phenol in the top layer. It is not labeled since the probability of finding is rather low. The water in this case acts as a proton donor H-bonds directly with the oxygen of phenol, similar to the dimer C in Fig. 4. The water molecules labeled with F, M and I in the middle and the top layers, as well as those with G, K and L in the bottom layer may be regarded as the water molecules in the second hydration shell. Their stabilization energies are to be from the caging effects.

The analysis of the MC results in the present section shows clearly that there exist quite well-defined networks of water molecules in the first hydration shell of phenol. The structural analysis made

here reveals a complete and understandable picture of the hydration structure of phenol in aqueous solution.

5. Molecular dynamics (MD) simulations of liquid phenol

Since the experimental results on dynamic properties of liquid phenol are restricted, the main aim of the NVE-MD simulations was only to investigate the structure of liquid phenol and compare it with available theoretical and experimental results of similar systems.

Liquid phenol was studied at 330 and 360 K. 216 phenol molecules were put in a cubic box subject to periodic boundary conditions. The density of liquid phenol was maintained at 1 g/cm^3 in the MD runs for all the above temperatures. The density corresponds to a box length of 32.3 Å. The cut-off radius was half of the box length. The long range Coulomb interactions were handled using the Ewald summation. The velocity scaling was used during the equilibration period. The time step selected to solve the equations of motion was 0.0005 ps. About 8000 MD steps were devoted to the equilibration at each temperature and additional 10000 steps for property calculations. The structural properties of interest were the atom–atom pair correlation functions ($g(R)$) and the running coordination numbers ($n(R)$) of molecules in the first solvation sphere. The dynamic property considered was the self-diffusion coefficient (D) which was derived from the velocity autocorrelation function. The MD program employed was MOLDY, written and maintained by Refson [43]. The routine for the calculation of forces in MOLDY was modified by the present authors to handle the T-model potential.

The calculated potential energies and pressures of liquid phenol at various temperatures are listed in Table 4. The potential energy of liquid phenol derived from MD at 334 K is −55.55 kJ/mol, which is in line with the experimental ΔH_{vap} for liquid phenol at 298 K of 57.82 kJ/mol [44]. Good agreement with the experimental result is partially due to the calibration of the T-model potential to the experimental $B(T)$ through C_6. The averaged pressures during the MD simulations, on the other hand, are rather high. This is due to the fact that the pressure is a quantity which is sensitive to the detail on the potential energy surface. In the case of liquid benzene [9], the averaged pressures during the MD simulations varies from −70 to 1500 atm, depending on the force fields used. It was also shown in Ref. [9] that the computed pressures could be improved by extending the truncation distance. This helps reduce the truncation error. For the present work, this can be done by increasing the box length and the number of molecules in the box. This will surely require more computational resources for the MD simulations. Since the pressure was not the main focus here, we gave no further consideration in improving the values of the averaged pressures.

Table 4
The averaged potential energies (ΔE_{pot}), pressures (P) and self-diffusion coefficients (D) of liquid phenol derived from MD

T (K)	ΔE_{pot} (kJ/mol)	P (atm)	D (10^{-5} cm^2/s)
334	−55.55	252	0.75
362	−52.84	569	1.36

For the structural properties, the peak heights and positions of $g(R)$ at various temperatures were quite similar. Therefore, $g(R)$ are shown only at 334 K in Fig. 6. Since the H-bonding is one of the most important binding features in liquid phenol, the discussion on the liquid structure will be made based mainly on $g(R_{OO})$ and $g(R_{OH})$. The interpretation of $g(R)$ will be supported by the characteristic distances listed in Fig. 2. Since both $g(R_{OH})$ and $g(R_{CC})$ show nearly no structure, $g(R_{C1C1})$ and $g(R_{C4C4})$ were extracted from $g(R_{CC})$, and $g(R_{OH4})$ from $g(R_{OH})$ and included in Fig. 6.

In Fig. 6, $g(R_{OO})$ shows the main peak at 2.90 Å. This peak corresponds to the O–H...O H-bond distance, found in the phenol dimers A and B to be 2.97 Å. The integration of $g(R_{OO})$ to the first maximum and minimum yielded about 0.7 phenol molecule at the closest O...O distance, and about 2 phenol molecules at the O...O distance of 4 Å. Only two small humps are seen at 2.1 and 2.6 Å for $g(R_{OH})$. The former could be attributed easily to the O–H...O H-bond and the latter is the C–H...O H-bond interaction. $g(R_{OH4})$ shows two well-defined peaks at 2.1 and 3.5 Å, respectively. The first

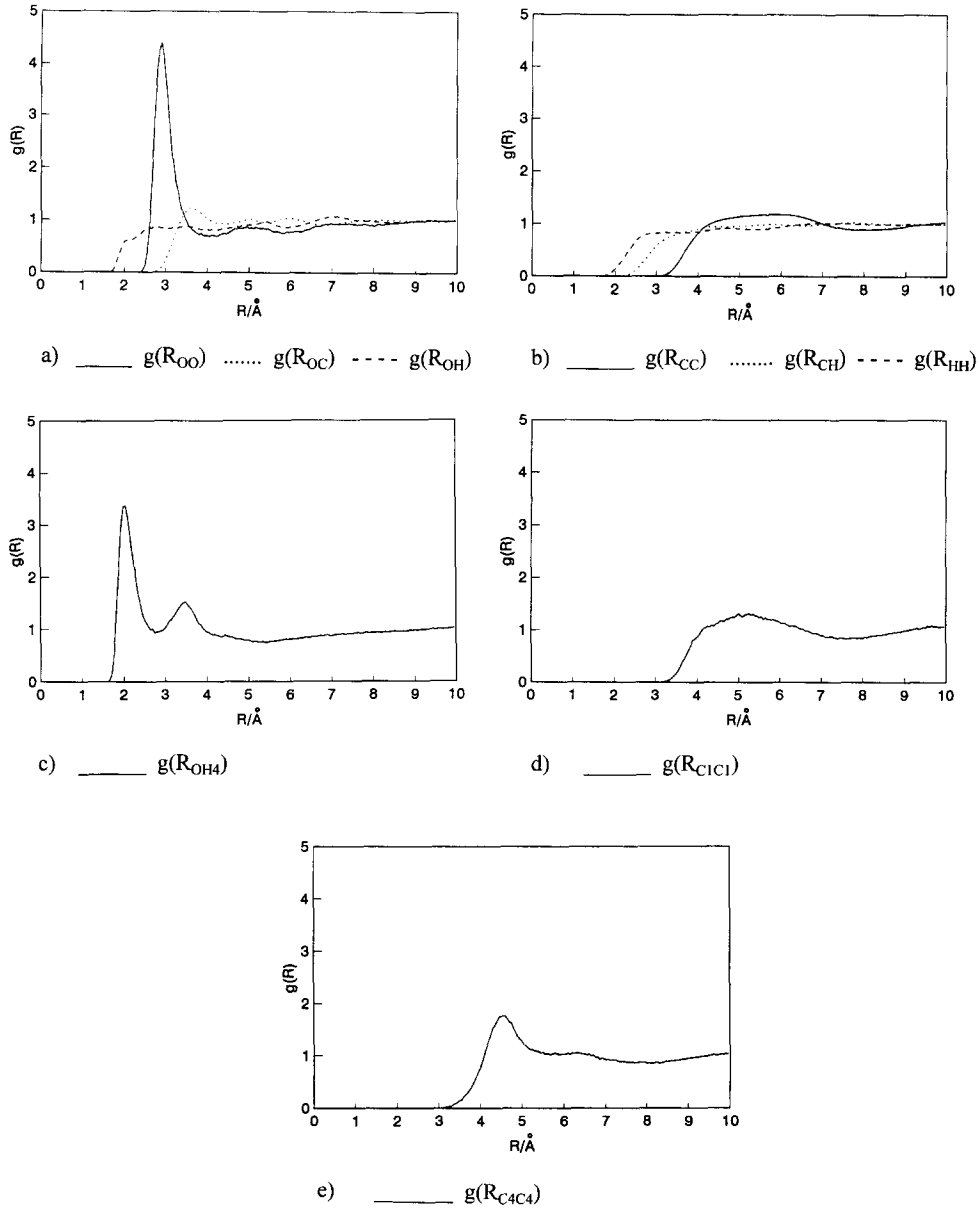

Fig. 6. Intermolecular pair correlation functions $g(R)$ for liquid phenol derived from MD at 334 K.

peak corresponds to the O...H distance found in the O–H4...O H-bonds and the second to another H4...O distance, not involved in H-bonding, see the dimers A and B in Fig. 2 for comparison. The integration of $g(R_{OH4})$ to the second maximum yielded 1.5 molecules of phenol at the O...H4 distance of 3.5 Å. The atom–atom pair correlation functions discussed up to this point suggest that the H-bond arrangements, similar to those in the dimers A and B, dominate in the liquid phenol. In order to determine the averaged orientation and the number of phenol molecules in the first solvation sphere

another approximation must be made. Since C4 stays quite near to the center of mass of phenol, C4 could be approximated to be the center of mass of phenol. $g(R_{C4C4})$ shows the main peak and a small shoulder at 4.5 and 6.5 Å, respectively. The first minimum corresponding to the size of the first solvation sphere is seen at 8.0 Å. The value is slightly larger than that of liquid benzene at 298 K, 7.5 Å [7]. The position of the main peak is slightly longer than the C4...C4 distance in the dimer A and slightly shorter than that in the dimer B. From this additional structural information, one expects that, on average, the orientation of phenol molecules in the liquid is somewhere between the dimer A and B. The integration of $g(R_{C4C4})$ to the position of the main peak yielded 1.33 molecules in closest contact, and to the first minimum yielded about 12.8 phenol molecules in the first solvation sphere. The latter is in good agreement with the results of liquid pyridine [17] and benzene [7], in which about 12 molecules were found in the first solvation sphere. One of the characteristic atom–atom distances of the cyclic trimer is the O...H4 distance of 2.96 Å, see Fig. 3. In the present study, there is no direct evidence from MD showing the existence of the cyclic trimers in the liquid.

The self-diffusion coefficients (D) derived from MD are included in Table 4. Since there is no experimental data on the self-diffusion coefficient for pure liquid phenol, the results in Table 4 will be discussed in comparison with some selected systems. The mutual-diffusion coefficients (D_{12}) in water–phenol mixture were studied in the temperature range of 296.5 to 343.0 K, using the Taylor dispersion technique [45]. The values of D_{12} were reported in the concentration range from infinite dilution to 8 wt-% phenol. Within this concentration range at 328 K, the experimental D_{12} varies from 1.75×10^{-5} to 0.85×10^{-5} cm^2/s. It was concluded in Ref. [45] that phenol molecules start to form aggregates in the bulk solution at the phenol weight fraction about 7–8 wt-%. At 330 K, the present MD predicted the self-diffusion coefficient to be 0.75×10^{-5} cm^2/s. The MD result seems to be in reasonable agreement with the experiment. The self-diffusion coefficient for pyridine was deduced from MD at 360 K to be 0.84×10^{-5} cm^2/s [17] which is lower than the value for liquid phenol at the same temperature, 1.36×10^{-5} cm^2/s.

6. Conclusion

In the present work, an intermolecular potential was constructed based on the T-model to describe the interaction between phenol molecules. The computed T-model potential was used in the investigation of structures and interaction energies of phenol dimers and trimers in the gas phase. The most probable equilibrium structure of phenol dimer was predicted by the T-model potential to be a H-bonded configuration, with the interaction energy of -31.31 kJ/mol. The result is in excellent agreement with the rotational coherence spectroscopic results, in which a similar dimer structure was detected in the gas phase. The most probable structure of the phenol trimer was suggested by the T-model potential to be a cyclic arrangement of the O–H...O H-bonds similar to the water trimer. This cyclic structure was previously found in a vibrational spectroscopic experiment, by the measurement of the Raman depolarization ratios. The absolute and some local minimum energy geometries of phenol dimers were partially checked by ab initio calculations with a DZ basis set at the MP2 level of theory, both with and without the counterpoise correction of BSSE. Good agreement between the T-model and MP2 results was obtained.

The T-model potential for phenol was combined with that of water to investigate the phenol–water 1:1 complex. The results were verified by MP2 calculations with a DZP basis and with the counterpoise correction. The T-model and the MP2 results, as well as the spectroscopic and molecular beam experiments, all indicated that the phenol–water 1:1 complex, in which water acts as a proton acceptor H-bonding to O–H4 of phenol, is the most stable form in the gas phase.

The T-model potentials to describe the interaction between phenol and water were further applied in the study of the hydration structure and energy of phenol in aqueous solution, using MC simulations at 298 K. The averaged positions, as well as the orientations, of water molecules in the first and second hydration shells of a phenol molecule were represented by the oxygen (PDO) and hydrogen probability distribution (PDH) maps, respectively. It was found that water molecules tend to concentrate and form H-bonded networks in the vicinity above as well as below the molecular plane of phenol. The analysis of the AWPD

and WWPD maps led to the conclusion that both solute–solvent and solvent–solvent interactions are responsible for the stability of water molecules in the first hydration shell. In the second hydration shell, however, only the solvent–solvent interaction is the most important factor in determining the hydration structures.

The T-model potential for phenol was applied in the MD simulations of liquid phenol at 330 and 360 K. The structural information inferred from the MD simulations suggested that liquid phenol is dominated by the O–H...O H-bonded structures, similar to those found in the dimers. The first-solvation sphere contains about 12 phenol molecules, within the radius of about 8.0 Å. There was no direct evidence showing the existence of the cyclic trimers in the liquid. The self-diffusion coefficients computed from MD are quite reasonable in comparison with the mutual-diffusion coefficients of phenol in aqueous solution at the limit at which phenol molecules start to form aggregates.

It should be emphasized that the results presented in this work were based on a pairwise additive scheme, in which the many-body effects are neglected. The many-body effects have been shown to be not negligible for many H-bonded systems, hydrogen fluoride as an example. The authors expect that they could also affect, more or less, the properties reported here. However, from the comparison of the present results with available theoretical and experimental data, the authors believe that the present results on structures, energetics and dynamics of liquid phenol as well as phenol in aqueous solution are quite reasonable. We hope that the present work will attract attention from experimentalists to investigate this system further.

Acknowledgements

We are indebted to the High-Performance Computer Center (HPCC) under the National Electronic and Computer Technology Center (NECTEC) in Bangkok for the CPU time on the Silicon Graphics Power Challenge and Cray YMP-El98 supercomputers. Large part of the calculations was performed on the DEC Alpha 4710 and DEC Alpha 600/5-266 at the School of Chemistry, Suranaree University of Technology, Thailand.

References

[1] J.M. Goodfellow (Ed.), Computer Modeling in Molecular Biology VCH, Weinheim, 1995.
[2] D.A. Smith (Ed.), Modeling of Hydrogen Bonds American Chemical Society, Washington, 1994.
[3] R.R. Dogonadze, E. Kalman, A.A. Kornyshev, J. Ulstrup (Eds.), The Chemical Physics of Solvation, part C, Elsevier, Amsterdam, 1988.
[4] N. Holberstadt, K.C. Janda (Eds.), Dynamics of Polyatomic and Van der Waals Complexes, NATO ASI series B: Physics Vol. 227, Plenum Press, New York, 1989.
[5] H. Halberland (Ed.), Clusters of Atoms and Molecules, Springer, Berlin, 1994.
[6] P.L. Huyskens, W.A.P. Luck, T. Zeegers-Huyskens (Eds.), Intermolecular Forces, Springer, Berlin, 1991.
[7] W.L. Jorgensen, D.L. Severance, J. Am. Chem. Soc. 112 (1990) 4768.
[8] E. Arunan, H.S. Gutowsky, J. Chem. Phys. 98 (1993) 4294.
[9] G.D. Smith, R.L. Jaffe, J. Phys. Chem. 100 (1996) 9624.
[10] P. Hobza, H.L. Selzle, E.W. Schlag, J. Am. Chem. Soc. 116 (1994) 3500.
[11] R.L. Jaffe, G.D. Smith, J. Chem. Phys. 105 (1996) 2780.
[12] S. Sun, E.R. Bernstein, J. Phys. Chem. 100 (1996) 13348.
[13] H.J. Boehm, R. Ahlrichs, J. Chem. Phys. 77 (1982) 2028.
[14] H.J. Boehm, C. Meissner, R. Ahlrichs, Mol. Phys. 53 (1984) 651.
[15] K.P. Sagarik, V. Pongpituk, S. Chiyapongs, P. Sisot, Chem. Phys. 156 (1991) 439.
[16] K.P. Sagarik, P. Asawakun, submitted for publication
[17] K.P. Sagarik, E. Spohr, Chem. Phys. 199 (1995) 73.
[18] K.P. Sagarik, R. Ahlrichs, S. Brode, Mol. Phys. 57 (1986) 1247.
[19] Y.P. Puhovski, B.M. Rode, Chem. Phys. 190 (1995) 61.
[20] K.P. Sagarik, R. Ahlrichs, J. Chem. Phys. 86 (1987) 5117.
[21] U.C. Singh, P.A. Kollman, J. Comput. Chem. 5 (1984) 129.
[22] D.E. Williams, J. Comput. Chem. 9 (1988) 745.
[23] N.W. Larsen, J. Mol. Struct. (Theochem) 51 (1979) 175.
[24] C.W. Bock, M. Trachtman, P. George, J. Mol. Struct. (Theochem) 139 (1986) 63.
[25] R.J.L. Andon, D.P. Biddiscombe, J.D. Cox, R. Handly, D. Harrop, E.F.G. Herington, J.F. Martin, J. Chem. Soc. (1960) 5246.
[26] L.L. Connell, S.M. Ohline, P.W. Joireman, T.C. Corcoran, P.M. Felker, J. Chem. Phys. 96 (1992) 2585.
[27] M.C. Moreau-Descoings, G. Goethals, J.P. Seguin, Bull. Soc. Chim. Belg. 97 (1988) 127.
[28] H.S. Gotowsky, T. Emilsson, E. Arunan, J. Chem. Phys. 99 (1993) 4883.
[29] S. Suzuki, P.G. Green, R.E. Bumgarner, S. Dasgupta, W.L. Goddard III, G.A. Blake, Science 257 (1992) 942.
[30] K.A. Peterson, T.H. Dunning Jr., J. Chem. Phys. 102 (1995) 2032.
[31] E. Clementi, Determination of Liquid Structure, in: Lecture Notes in Chemistry, Springer, Berlin, 1976, p. 69.
[32] M. Quack, J. Stohner, A. Suhm, J. Mol. Struct. 294 (1993) 33.

[33] T. Ebata, T. Watanabe, N. Mikami, J. Phys. Chem. 99 (1995) 5761.
[34] F. Ramondo, L. Bencivenni, G. Portalone, A. Domenicano, Struct. Chem. 6 (1995) 37.
[35] S. Chaiyapongs, Dissertation, Ramkhamhaeng University, Bangkok, 1995.
[36] M.J. Frisch, J.E. Del Bene, J.S. Binkley, H.F. Schaefer, J. Chem. Phys. 84 (1986) 2279.
[37] M. Schuetz, T. Buergi, S. Leutwyler, J. Chem. Phys. 98 (1993) 3763.
[38] D. Feller, M.W. Feyereisen, J. Comput. Chem. 14 (1993) 1027.
[39] E. Clementi, Computational Aspects for Large Chemical Systems, in: Lecture Notes in Chemistry 2, Springer, Berlin, 1980.
[40] K. Sagarik, G. Corongiu, E. Clementi, J. Mol. Struct. (Theochem) 235 (1991) 355.
[41] A. Pohorille, I. Bemjamin, J. Chem. Phys. 94 (1991) 5599.
[42] A. Ben-Naim, Y. Marcus, J. Chem. Phys. 81 (1984) 2016.
[43] K. Refson, Moldy User's Manual, Department of Earth Science, Oxford University, 1996.
[44] D.R. Lide (Ed.), CRC Handbook of Chemistry and Physics, 72th ed., CRC Press, Boca Raton, 1991.
[45] R. Castillo, C. Garza, J. Orozco, J. Phys. Chem. 96 (1992) 1475.